Microchimica Acta (2021) 188: 56
https://doi.org/10.1007/s00604-021-04705-4

ORIGINAL PAPER

Colorimetric determination of amyloid-β peptide using MOF-derived nanozyme based on porous ZnO-Co_3O_4 nanocages

Xi Zhou[1] · Shuangling Wang[1] · Cong Zhang[2] · Yulong Lin[1] · Jie Lv[1] · Shuyang Hu[1] · Shanshan Zhang[1] · Meng Li[1]

Received: 28 September 2020 / Accepted: 9 January 2021 / Published online: 27 January 2021

Abstract

A sensitive and rapid colorimetric biosensor has been developed for determination of amyloid-β peptide (Aβ) and study of amyloidogenesis based on the high peroxidase-like activity of porous bimetallic ZnO-Co_3O_4 nanocages (NCs). Due to the high binding ability of Aβ monomer to ZnO-Co_3O_4 NCs, the catalytic activity of ZnO-Co_3O_4 NCs can be significantly suppressed by Aβ monomer. This finding forms the basis for a colorimetric assay for Aβ monomer detection. The detection limit for Aβ monomer is 3.5 nM with a linear range of 5 to 150 nM ($R^2 = 0.997$). The system was successfully applied to the determination of Aβ monomer in rat cerebrospinal fluid. Critically, the different inhibition effects of monomeric and aggregated Aβ species on the catalytic activity of ZnO-Co_3O_4 NCs enabled the sensor to be used for tracking the dynamic progress of Aβ aggregation and screening Aβ inhibitors. Compared with the commonly used thioflavin T fluorescence assay, this method provided higher sensitivity to the formation of Aβ oligomer at the very early assembly stage. Our assay shows potential application in early diagnosis and therapy of Alzheimer's disease (AD).

Keywords Porous ZnO-Co_3O_4 nanocages · Peroxidase-like activity · Amyloid-β peptide · Amyloidogenesis study · Inhibitor screening · Alzheimer's disease

Introduction

Aggregation of amyloid-β peptide (Aβ) into oligomers, fibrils and plaques is one of the main hallmarks in the early onset of Alzheimer's disease (AD) [1–3]. Sensitive monitoring the aggregation process of Aβ and screening inhibitors of Aβ aggregation have been reported to be significantly important for the diagnosis and therapy of AD [4,5]. Until now, inhibitors against Aβ aggregation as potential AD therapeutics have been widely developed [2]. However, the methods for monitoring the aggregation process of Aβ and screening Aβ inhibitors are less reported, which can hinder the discovery of Aβ inhibitors. The mainly used analysis methods include surface-enhanced Raman spectroscopy [6], mass spectrometry [7], enzyme-linked immunosorbent assay [8], and fluorescent probes [5]. Although promising, most of these methods are low-throughput, time-consuming, and always dependent on an extensive and expensive instrumentation, leading them not practically suitable for high-throughput screening of Aβ inhibitors. Among these methods, utilizing fluorescent probes is superior in terms of simplicity, rapidity, and low cost. Thioflavin T (ThT), the commonly used amyloid dye, is the most standardized way to monitor amyloid [9]. However, ThT fluorescence assay shows some fatal drawbacks, such as a small stokes shift, low sensitivity, and false-positive response [10]. Most importantly, owing to its specific binding to β-sheet rich structure, ThT fluorescence is only responsive to the fibrils of Aβ and insensitive to the monomers and intermediates especially the most toxic Aβ oligomers, leading to the unsuitability for quantitative and kinetic study [10].

In addition to the fluorescence assay, colorimetric assay in which the readout can be visualized using the naked eye has also become an effective route in clinical diagnosis [11,12]. However, up to date, the colorimetric method for monitoring the entire aggregation process of Aβ from monomer to fibril

Xi Zhou and Shuangling Wang contributed equally to this work.

✉ Cong Zhang
zhangcong0672@163.com

✉ Meng Li
limeng87@hotmail.com

[1] College of Pharmacy, Hebei Medical University, Shijiazhuang 050017, China

[2] Department of Chemistry, School of Sciences, Hebei University of Science and Technology, Shijiazhuang 050018, China

and screening Aβ inhibitors has been rarely reported. Therefore, there is an increasing demand to develop novel colorimetric assays for sensitively monitoring Aβ aggregation and screening Aβ inhibitors especially the inhibitors against the formation of soluble Aβ oligomers.

Metal organic frameworks (MOFs), as a kind of porous crystalline materials, are built by the self-assembly of metal node and organic linker [13]. With the advantage of facile synthesis, high surface area, ordered porosity, and multifunctionalities, MOFs have attracted considerable interest and been widely applied in the fields of photocatalysis, separation, biomedicine, energy conversion, and storage [13,14]. Recently, MOFs with catalytically active metal nodes have been reported to exhibit enzyme-like catalytic activity, which extends their applications in environmental detection and biomedical field [15,16]. However, due to the nature of noncovalent bond in the formation of MOFs, MOFs can be gradually decomposed via ligand exchange reactions with monodentate ligands in biological systems [17], making them unsuitable to establish biosensors for disease diagnosis. Using MOFs as templates or sacrificial precursors to prepare new porous materials with high stability can be a promising strategy to overcome these limitations of MOFs [18,19]. The resulting MOF derivatives which maintain the tailorable porous structures, large surface areas, and numerous active sites of the parent MOFs [18,19] can expose all the active sites as far as possible to the substrates [20]. Therefore, the MOF derivatives can be promising candidates to construct nanozyme-based biosensors. Most recently, nanozyme, a type of nanomaterial with intrinsic enzyme-like activity, has been reported to exhibit great application potentials in developing biosensors for Aβ detection due to the high stability and adjustable catalytic activity [11,21].

Herein, porous bimetallic transition metal oxide nanocage (ZnO-Co_3O_4 NC) via the facile oxidation of ZnCo-zeolitic-imidazolate-framework (ZnCo-ZIF) [19] was prepared as a novel probe for Aβ detection and amyloidogenesis study. Similar with the reported bimetallic MOFs [20], the obtained ZnO-Co_3O_4 NCs possess intrinsic peroxidase-like activity. Compared with the single metal-based nanomaterials, the porous bimetal nanomaterials have strong catalytic activity due to the synergistic effect of bimetals [22]. It is well-known that the metal ions including Zn^{2+} and Co^{3+} exhibit a high binding affinity with Aβ monomers [23,24]. The interaction between Aβ monomers and these metal ions can enthalpically drive initial adsorption of Aβ onto the surface of the nanocages [25]. Binding of Aβ onto the surface of nanocages can significantly block or shield the active sites of ZnO-Co_3O_4 NCs, thereby suppressing the peroxidase-like activity of ZnO-Co_3O_4 NCs. After Aβ assembled, the obtained Aβ aggregates show a lower binding ability to ZnO-Co_3O_4 NCs than Aβ monomer, leading to a decreased inhibition effect on the catalytic activity of ZnO-Co_3O_4 NCs (Scheme 1). On the basis of the different inhibition effects of these Aβ species (including Aβ monomers, Aβ oligomers, and Aβ fibrils) on the peroxidase-mimicking activity of ZnO-Co_3O_4 NCs, our colorimetric assay can sensitively monitor the entire aggregation process of Aβ and screen Aβ inhibitors.

Experimental section

Reagents and materials

Hydrochloric acid (HCl, 36–38%) was purchased from Sinopharm Chemical Reagent Co., Ltd. (China, http://www.reagent.com.cn). 3,3′,5,5′-Tetramethylbenzidine (TMB, > 98%) was obtained from Adamas-beta (Shanghai, China, http://www.adamas-beta.com). Sodium hydroxide (NaOH, ≥ 96%) was purchased from Tianjin Fengchuan Chemical Reagent Technologies Co., Ltd. (Tianjin, China, http://www.tjhxsj.cn). Arginine (Arg, ≥ 99%), cysteine (Cys, ≥ 99%), glycine (Gly, ≥ 99%), histidine (His, ≥ 99%), serine (Ser, ≥ 99%), threonine (Thr, ≥ 99%), tyrosine (Tyr, ≥ 99%), bovine serum albumin (BSA, ≥ 98%), dimethyl sulfoxide (DMSO, ≥ 99.9%), thioflavin T (ThT, ≥ 98%), curcumin (> 98%), $Co(NO_3)_2{\cdot}6H_2O$ (≥ 99%), $Zn(NO_3)_2{\cdot}6H_2O$ (≥ 99.9%), and 2-methylimidazole (≥ 98%) were supplied by Aladdin Ltd. (Shanghai, China, http://www.aladdin-e.com). Hydrogen peroxide (H_2O_2, ≥ 30%) was obtained from Beijing Chemicals (Beijing, China, http://www.crc-bj.com). β-Cyclodextrin (β-CD, ≥99%) was purchased from Tianjin Yongda Chemical Reagent Co., Ltd. (Tianjin, China, http://www.tjydhxsj.com). Amyloid-β (1-40) (≥ 97%) was bought from Enzo (New York, USA, https://www.enzo.com). Glucose (≥ 99.5%) was bought from Sigma-Aldrich (St. Louis, MO, USA, https://www.sigmaaldrich.com). 1,1,1,3,3,3-Hexafluoro-2-propanol (HFIP, ≥ 99%) was purchased from J&K Chemical Ltd. (Beijing, China, http://www.jkchemical.com). All the reagents in our study were not further purified and used as-received.

Methods

Powder X-ray diffraction patterns were monitored on a Bruker AXS D8 Advance diffractometer (Cu-Kα radiation, λ = 1.5406 Å, https://www.bruker.com/). The UV-vis absorption spectra were recorded with the TU-1950 spectrophotometer (Beijing Purkinje General Instrument Co., Ltd., http://www.pgeneral.com/). Transmission electron microscopy (TEM) images were taken using a Hitachi H-7650B microscope operating at 200 kV (Japan, https://www.hitachi-hightech.com/global/). Fourier transform infrared spectroscopy (FTIR) analysis was performed on a BRUKER Vertex 70 FTIR spectrometer (Germany, https://www.bruker.com/). Scanning electronic microscopy (SEM) images were captured using a Hitachi S-4800 (Japan,

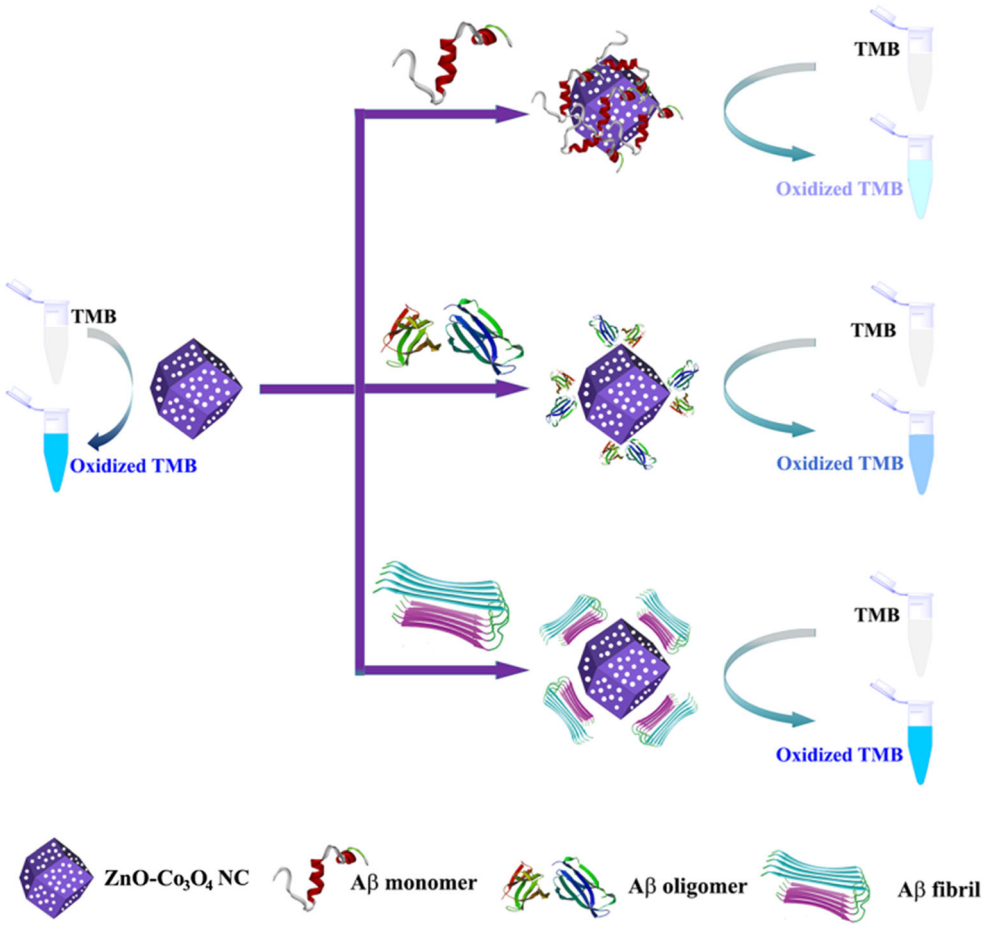

Scheme 1 Schematic illustration of utilizing ZnO-Co_3O_4 NCs as nanozymes for colorimetric detection of Aβ and amyloidogenesis study

https://www.hitachi.com/). A FEI Tecnai G2 F30 microscope equipped with an energy-dispersive X-ray spectrometer (EDS) was used to obtain high-resolution TEM (HRTEM) images and the elemental mapping results (USA, https://www.fei.com/).

Sample preparation

Aβ40 stock solution was prepared according to the previous reports [10]. Briefly, the powered Aβ peptide was first dissolved in HFIP. The solution was shaking at 4 °C for 2 h in a sealed vial for further dissolution and then stored at − 20 °C as a stock solution. Before use, HFIP was removed by evaporation under a gentle stream of nitrogen, and the peptide was dissolved in water. The concentration of monomeric Aβ was determined by UV absorbance with a calculated extinction coefficient of 1450 cm^{-1} M^{-1} at 276 nm. The Aβ40 oligomer or fibril solution concentration was calculated as the equivalent concentration to Aβ40 monomer.

Characterization of interaction of ZnO-Co_3O_4 NCs with Aβ

To demonstrate the different binding ability of Aβ monomers, Aβ oligomers, and Aβ fibrils with ZnO-Co_3O_4 NCs, Aβ species (200 μM) in PBS (50 μL, pH 5.0) were mixed with ZnO-Co_3O_4 NCs (30 μg), and then incubated for 10 min at 37 °C. The mixture was centrifuged and washed with PBS. The supernatant was collected and used for UV-vis absorbance detection.

Detection of Aβ

For the detection of Aβ monomer, 4 μL ZnO-Co_3O_4 NCs (2 $mg{\cdot}mL^{-1}$) and 4 μL different concentrations of Aβ monomer (0, 0.001, 0.005, 0.01, 0.025, 0.05, 0.075, 0.1, 0.15, 0.25, 0.4, 0.5, 0.74, 1.0, 1.25, 1.5, 2.0 μM) were incubated in PBS buffer (pH 5.0, 384 μL) for 10 min. After that, 4 μL TMB (42 mM), and 4 μL H_2O_2 (1 M) were successively added into the solution. The mixture was further incubated at room temperature for 5 min, and then the UV-vis absorption spectra of the solution were monitored. To monitor the aggregation of Aβ, Aβ monomers were incubated in the aggregation buffer (10 mM Tris in 150 mM NaCl, pH 7.3) at 37 °C for different days (0–7 days). And then, the same experiments were carried out. The final concentration of Aβ was 1 μM. The data of ThT fluorescence and the absorption of the system of ZnO-Co_3O_4 NCs/H_2O_2/TMB were normalized to their maximum, respectively. Each experiment was replicated in triplicate. The

selectivity of this assay for Aβ monomer detection was examined by comparing the responses of Aβ monomer with different biomolecules including Arg, His, Tyr, Gly, Cys, Ser, Thr, glucose, and BSA. The concentration of glucose and BSA was 10 μM and 5 μM for other amino acids. To detect Aβ monomer in the presence of cerebrospinal fluid (CSF), the rat CSF was diluted 1:50 in PBS (pH 5.0) and used in 1 day after dilution. Then the same experiments were carried out using the diluted CSF instead of PBS.

Screening Aβ inhibitors

To screen Aβ inhibitors, 100 μM Aβ solutions in the presence of 100 μM ligands were incubated at 37 °C for different days (0–7 days) in aggregation buffer (10 mM Tris in 150 mM NaCl, pH 7.3). Then the same experiments as that for detection of Aβ were carried out. As controls, the effects of the ligands on the peroxidase-like activity of ZnO-Co_3O_4 NCs were also detected. The data of the absorption of the system of ZnO-Co_3O_4 NCs/H_2O_2/TMB was normalized to the maximum absorbance intensity of the sample without Aβ inhibitors. Each experiment was replicated in triplicate.

Results and discussion

Characterizations of ZnO-Co_3O_4 NCs

To develop this strategy, ZnO-Co_3O_4 NCs were synthesized via the facile oxidation of ZnCo-ZIF [19]. As shown in Fig. S1A and Fig. S1B, the parent ZnCo-ZIF nanocrystals are monodispersed with an average size of ~ 230 nm. After calcination, the hollow rhombic polyhedral morphology is maintained, whereas the surface becomes wrinkled, according to the SEM and TEM images (Fig. S1C and Fig. S1D). The formations of ZnO-Co_3O_4 NCs were also validated by XRD analysis (Fig. S1E) and FTIR spectra (Fig. S1F) [26]. The HRTEM images and TEM elemental-mapping images for ZnO-Co_3O_4 reveal that Zn and Co are homogeneously distributed (Fig. S2). Thermogravimetric analysis indicates the high thermal stability of the obtained ZnO-Co_3O_4 NCs (Fig. S3A). N_2 adsorption-desorption isotherms of ZnO-Co_3O_4 NCs show a typical type IV curve with an average pore diameter of 9.7 nm (Fig. S3B). The porous structure would increase the diffusion of reaction substrate in and out of the nanocages, which can significantly enhance the catalytic activity of ZnO-Co_3O_4 NCs. All these results demonstrate that the ZnO-Co_3O_4 NCs have been synthesized successfully.

Peroxidase-like activity of ZnO-Co_3O_4 NCs

With the confirmation of the successful fabrication of ZnO-Co_3O_4 NCs, the peroxidase-like activity of ZnO-Co_3O_4 NCs was then evaluated via the oxidation of TMB by H_2O_2. As shown in Fig. 1a, in the presence of H_2O_2, the oxidation of TMB can be catalyzed by ZnO-Co_3O_4 NCs, which is accompanied by a color change of the solution from colorless to blue. The produced oxidized TMB shows a characteristic absorption peak at 652 nm. In contrast, the reaction solution does not exhibit any color change without ZnO-Co_3O_4 NCs (Fig. 1a), revealing the intrinsic peroxidase-like activity of ZnO-Co_3O_4 NCs. Interestingly, under the experimental condition, ZnO-Co_3O_4 NCs themselves can also induce the oxidation of TMB, which indicates that the obtained ZnO-Co_3O_4 NCs possess dual enzyme-like activities, peroxidase-like activity, and oxidase-like activity. However, the oxidase-like activity of ZnO-Co_3O_4 NCs is quite lower than their peroxidase-like activity (Fig. 1a). Therefore, the colorimetric assay for monitoring Aβ aggregation and inhibitor screening is established on the basis of the peroxidase-like activity of ZnO-Co_3O_4 NCs. The catalytic activity of ZnO-Co_3O_4 NCs is strongly dependent on pH value but not affected obviously by temperature (Fig. 1b and Fig. S4). Besides, an increased absorbance intensity at 652 nm was observed with the steady increase of the concentration of ZnO-Co_3O_4 NCs (Fig. S5). Considering the further physiological application as well as the appropriate catalytic performance, the optimal pH and temperature were chosen as pH 5.0 and 25 °C. The concentration of ZnO-Co_3O_4 NCs was chosen as 20 $\mu g \cdot mL^{-1}$.

To demonstrate the excellent catalytic activity of the porous bimetallic transition metal oxide nanocages, we also examined the activity of ZnO nanocages (ZnO NCs) and Co_3O_4 nanocages (Co_3O_4 NCs) which were synthesized using the same method. As shown in Fig. S6, Co_3O_4 NCs exhibit lower peroxidase-like activity than the same amount of ZnO-Co_3O_4 NCs, while ZnO NCs play a negligible role in the color reaction. The enhanced catalytic ability might result from the good dispersion of ZnO-Co_3O_4 NCs in aqueous solution (Fig. S7) and the decreased charge recombination by the formed heterostructures [27].

The catalytic mechanism of ZnO-Co_3O_4 NCs was also investigated by the steady state kinetic study [11]. As illustrated in Fig. 2, typical Michaelis-Menten curves were obtained within the suitable range of either H_2O_2 concentrations or TMB concentrations. The apparent Michaelis-Menten constant (K_m) and maximum initial velocity (V_{max}) were calculated with Lineweaver-Burk plot (Table 1). As indicated in Table 1, the K_m values of ZnO-Co_3O_4 NCs for H_2O_2 and TMB are close to that of HRP [20], indicating that ZnO-Co_3O_4 NCs exhibit an excellent catalytic efficiency, which is very close to that of natural HRP enzyme. Critically, compared with the monometallic Co_3O_4 NCs, the K_m values of ZnO-Co_3O_4 NCs for both H_2O_2 and TMB are lower than those of Co_3O_4 NCs, suggesting that the synergistic effects of the different active metals enhance the binding affinity with H_2O_2 and TMB. All these results suggest that ZnO-Co_3O_4

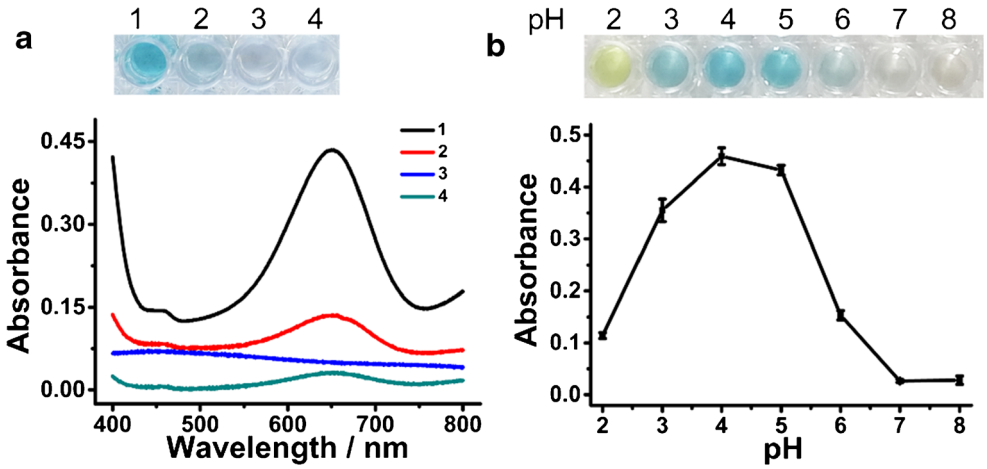

Fig. 1 The peroxidase mimetic properties of ZnO-Co_3O_4 NCs. **a** The absorption spectra of oxidized TMB in different reaction systems: (1) ZnO-Co_3O_4 NCs + H_2O_2 + TMB, (2) ZnO-Co_3O_4 NCs + TMB, (3) ZnO-Co_3O_4 NCs + H_2O_2, (4) H_2O_2 + TMB in PBS (pH 5.0) at room temperature after 5 min incubation. Above were the visual color changes of TMB in the corresponding solutions. **b** The influence of pH value on the catalytic activities of ZnO-Co_3O_4 NCs

NCs possess better catalytic activity than that of single-metal catalyst, making them extremely suitable to construct nanozyme-based sensors.

Detection of Aβ monomers via the ZnO-Co_3O_4 NC–based assay

To investigate whether ZnO-Co_3O_4 NCs can adsorb Aβ monomers, Aβ monomers were incubated with ZnO-Co_3O_4 NCs in solution. The efficiency of Aβ monomer bound to ZnO-Co_3O_4 NCs was calculated from the different absorbance intensities at 276 nm between the Aβ monomer solution before and after incubation with ZnO-Co_3O_4 NCs, which was determined to be 65.99 μmol·g^{-1} ZnO-Co_3O_4 NCs (Fig. S8A). Owing to the strong binding affinity with ZnO-Co_3O_4 NCs, Aβ monomer can significantly block the active sites in ZnO-Co_3O_4 NCs, leading to the reduced catalytic activity of ZnO-Co_3O_4 NCs. The ZnO-Co_3O_4 NC catalytic chromogenic system can be applied to detect Aβ monomer. In the present study, Aβ40, the most abundantly produced Aβ isoform, was chosen as the protein model, which has been widely used for in vitro amyloidogenesis study [10]. As shown in Fig. 3a, pre-incubation with Aβ40 monomers can obviously suppress the catalytic activity of ZnO-Co_3O_4 NCs. Along with the increase of the Aβ40 monomer concentration from 0 to 2 μM, the absorption of oxidized TMB at 652 nm gradually decreased while the color faded. The absorption intensities and the concentration of Aβ40 monomer show a good linear relationship in the range of 5 to 150 nM (Fig. 3b). The linear regression equation is $y = 0.430–0.390x$, and the correlation coefficient is $R^2 = 0.997$. Based on the equation limit of detection (LOD) = $3\sigma/m$ (σ is the standard deviation of the intercept and m is the

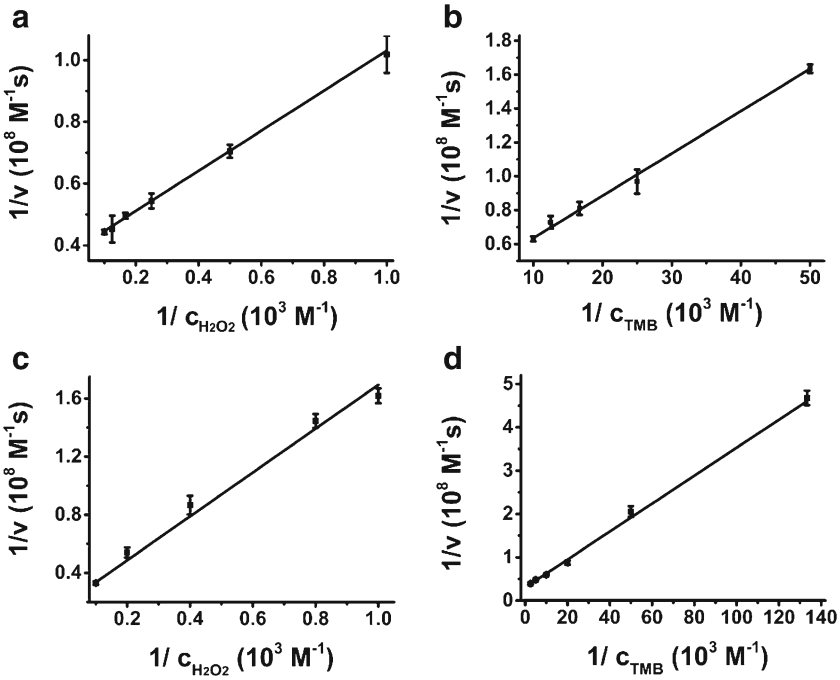

Fig. 2 Steady-state kinetic assay of ZnO-Co_3O_4 NCs or Co_3O_4 NCs. Lineweaver-Burk plot of the reciprocals of initial rate vs. substrate concentration for the determination of kinetic parameters K_m and V_{max} of ZnO-Co_3O_4 NCs (**a** and **b**) and Co_3O_4 NCs (**c** and **d**) with H_2O_2 (left) or TMB (right) as the substrate. Error bars were estimated from three independent measurements

Table 1 Comparison of the apparent Michaelis-Menten constant (K_m) and maximum reaction rate (V_{max}) between ZnO-Co_3O_4 NCs and Co_3O_4 NCs

Catalyst	Substrate	K_m (mM)	V_{max} (10^{-8} MS^{-1})
HRP[20]	H_2O_2	3.7	8.71
ZnO-Co_3O_4 NCs	H_2O_2	1.70	2.62
Co_3O_4 NCs	H_2O_2	8.15	5.41
HRP[20]	TMB	0.434	10
ZnO-Co_3O_4 NCs	TMB	0.065	2.63
Co_3O_4 NCs	TMB	0.11	3.31

slope of the calibration plot), the LOD was calculated to be 3.53 nM, which can meet the detection requirement of Aβ monomer level (nM) in cerebrospinal fluid (CSF) [28]. Compared with other previously reported nanomaterial-based methods (Table 2) [12,29–32], the colorimetric assay for detecting Aβ40 monomer presented in this article exhibits not only a comparable detection limit but also a fast response ability.

To demonstrate the specificity of the colorimetric assay for Aβ40 monomer detection, the influence of other amino acids and proteins especially those abundantly exist in human body was evaluated. As shown in Fig. 4a and Fig. 4b, no noticeable absorbance change was observed from the sample containing Arg, His, Tyr, Gly, Ser, Thr, glucose, and BSA even at a concentration much greater than that of Aβ40 monomer. For Cys, although a slight absorbance change was investigated upon addition of Cys, its concentration in CSF samples is lower than its present concentration (5 μM) [33]. After reducing the concentration of Cys, the interference was significantly reduced (Fig. S9). All these results indicate that the assay exhibits a high selectivity for Aβ40 monomer detection.

With the high selectivity toward Aβ40 monomer, we next evaluated whether the system can be used for detection of Aβ40 monomer in rat CSF, which is critical for AD diagnosis. As demonstrated in Fig. 4c, the absorption of oxidized TMB gradually decreased with the increase of the Aβ40 monomer concentration. The calibration curves present a linear relationship between the absorbance intensities and Aβ40 monomer concentration in the range of 5 to 150 nM with a detection limit of 1.58 nM in CSF (Fig. 4d). The linear regression equation is $y = 0.426–0.443x$, and the correlation coefficient is $R^2 = 0.998$. In addition, the analytical recoveries from the colorimetric method for Aβ40 monomer in CSF were 92.52%–107.6% with the relative standard deviations (RSDs, $n = 4$) between 2.61% and 3.72% (Table S1). The outcomes exhibit an encouraging conclusion that our system can be utilized for qualitative detection of Aβ40 monomer in CSF with good recovery and precision.

Monitoring Aβ aggregation via the ZnO-Co_3O_4 NC–based assay

It is well-known that as the disease progresses, Aβ monomers can gradually self-assemble into neurotoxic soluble oligomers and further the insoluble fiber filaments [1–3]. Based on this, it is of great importance to evaluate whether the ZnO-Co_3O_4 NCs' catalytic chromogenic system can discriminate Aβ oligomer or fibrils from Aβ monomer to monitor the aggregation process of Aβ. To verify this hypothesis, Aβ40 oligomers or fibrils were obtained via pre-incubation of Aβ40 stock solution in aggregation buffer at 37 °C for 2 days or 7 days, respectively. As indicated in Fig. 5a, pre-treatment with Aβ40 fibrils showed only a negligible inhibition effect on ZnO-Co_3O_4 NCs-catalyzed oxidation of the TMB-H_2O_2 system, while, in the existence of Aβ40 oligomers, the catalytic activity of ZnO-Co_3O_4 NCs was slightly decreased, but not as obvious as that induced by Aβ40 monomers (Fig. 5a).

When soft Aβ40 oligomers and Aβ40 fibrils are adsorbed on the surface of ZnO-Co_3O_4 NCs, the catalytic activity of ZnO-Co_3O_4 NCs can be inhibited to varying degrees. The different inhibition effects may arise from the different binding affinities between these Aβ40 species and ZnO-Co_3O_4 NCs. To verify our assumptions, we first quantitatively determined the binding efficiency of different Aβ40 species with ZnO-Co_3O_4 NCs. As displayed in Fig. S8, the Aβ bound efficiency was determined to be 65.99 μmol·g^{-1} ZnO-Co_3O_4 NCs for Aβ monomer, 39.63 μmol·g^{-1} ZnO-Co_3O_4 NCs for

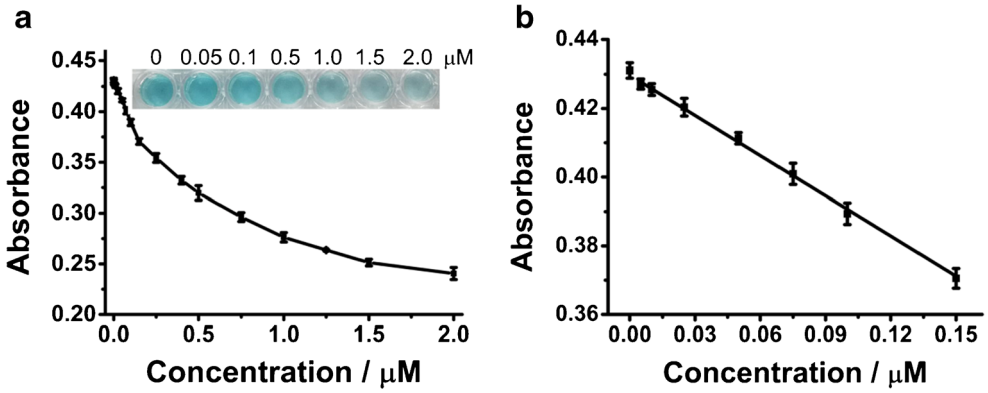

Fig. 3 Quantitative detection of Aβ monomer by ZnO-Co_3O_4 NC–based nanozyme. **a** The absorbance of the reaction solutions at 652 nm versus the concentration of Aβ monomer. **b** The linear plots of absorbance measured at 652 nm as a function of the concentration of Aβ monomer (mean ± SD, $n = 3$ for each sample)

Table 2 An overview on recently reported nanomaterial-based assays for detection of Aβ

Material-based	LOD (nM)	Detection range (nM)	Analytic time (min)	References
AuNP-based colorimetry	10.0	35.0 to 700	3	[29]
Prussian blue nanoparticle–based fluorescence	1	1 to 100	60	[30]
Polydopamine nanosphere–based fluorescence	12.5	20 to 10,000	40	[31]
Zn zeolitic imidazole framework–based colorimetry	500	500 to 100,000	25	[12]
Molybdenum disulfide nanosheet–based fluorescent	3.1	10 to 20,000	50	[32]
ZnO-Co_3O_4 NC–based colorimetry	3.53	5 to 150	15	This work

Aβ oligomer, and 19.04 μmol·g^{-1} ZnO-Co_3O_4 NCs for Aβ fibril. The order of the adsorption efficiency is Aβ40 monomer > Aβ40 oligomer > Aβ40 fibril, leading to the results that Aβ40 monomer shows the highest inhibitory effect on the catalytic activity of ZnO-Co_3O_4 NCs.

The distinct catalytic behaviors of ZnO-Co_3O_4 NCs with monomeric and aggregated forms of Aβ40 prompted us to explore the possibility to utilize ZnO-Co_3O_4 NCs for amyloidogenesis study. To monitor the aggregation process of Aβ40, the catalytic activity of ZnO-Co_3O_4 NCs in the presence of Aβ40 samples which were pre-incubated for different days was investigated. As depicted in Fig. 5b, with increasing incubation time of Aβ40 in aggregation solution, the absorption of the system at 652 nm was gradually increased. The absorbance changes at 652 nm exhibit a typical sigmoidal curve toward the incubation time (Fig. 5b), which is quite similar with the behavior of ThT, the commonly used amyloid fluorescence dye [9] (Fig. 5b). These results are

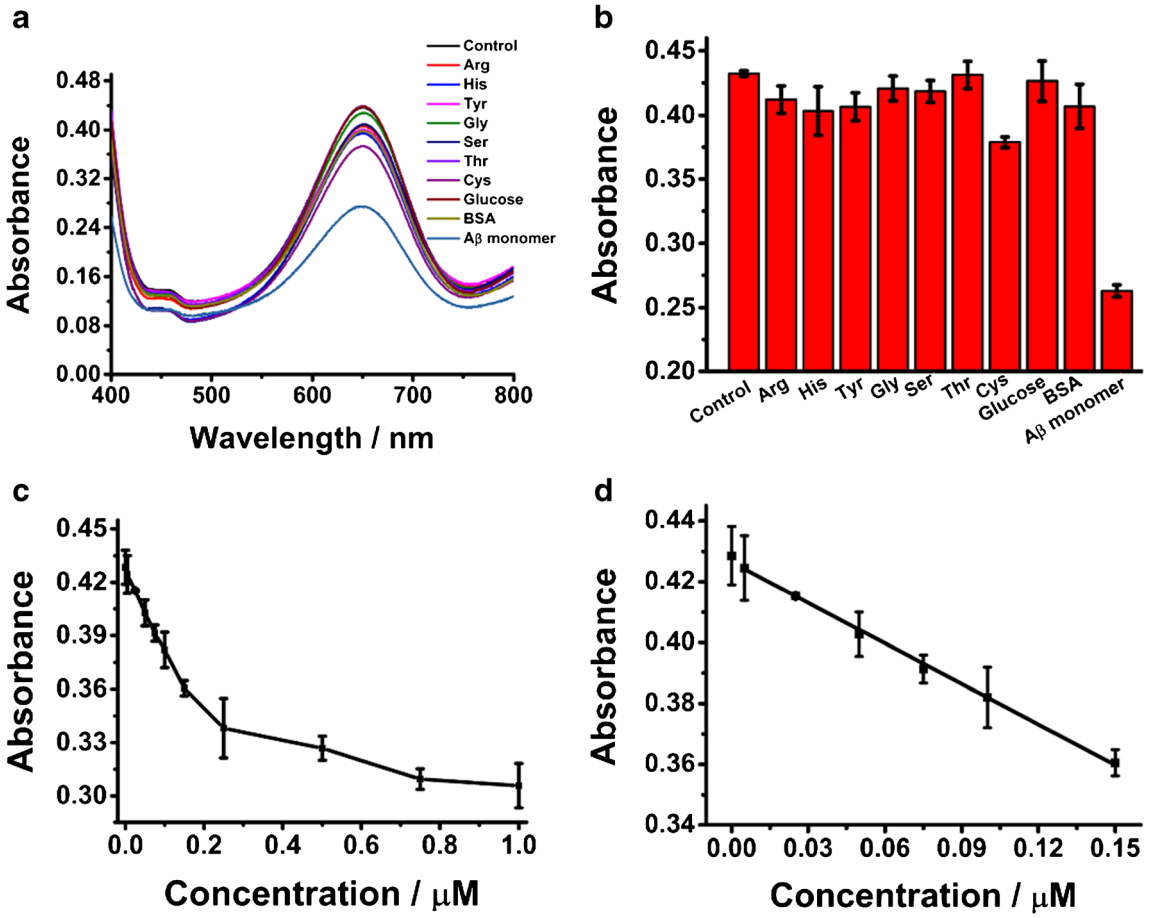

Fig. 4 **a** The absorbance spectra of TMB in the reaction systems of ZnO-Co_3O_4 NCs/H_2O_2 in the presence of potential interferences. **b** The absorption intensity at 652 nm of the reaction solution after the introduction of different biomolecules. **c** Detection of Aβ monomer in the presence of rat CSF. **d** The linear plots of absorbance measured at 652 nm as a function of the Aβ monomer concentration in rat CSF (mean ± SD, $n = 3$ for each sample)

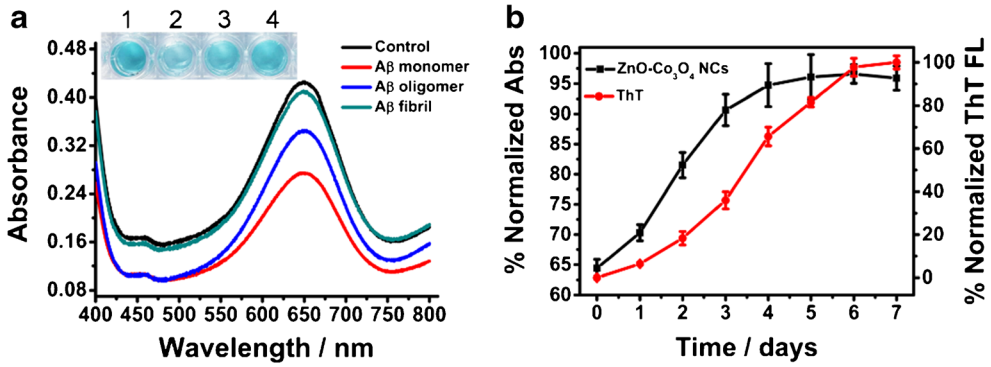

Fig. 5 **a** The UV-vis absorption spectra of the ZnO-Co_3O_4 NCs/H_2O_2/TMB solutions in the presence of Aβ monomer, oligomer, and fibril. Above were the visual color changes of the corresponding solutions: (1) control, (2) Aβ monomer, (3) Aβ oligomer, and (4) Aβ fibril. **b** Aβ fibrillogenesis process monitored by the ZnO-Co_3O_4-based method and ThT fluorescence assay. The plot of the absorbance measured at 652 nm and fluorescence intensity change of ThT against incubation time. The concentration of Aβ was 1 μM. The data of ThT fluorescence and the absorption of the ZnO-Co_3O_4 NC–based system were normalized to their maximum, respectively

consistent with nucleation-dependent polymerization model, indicating that ZnO-Co_3O_4 NCs possess the potentials in detection and kinetic study of Aβ40 aggregation. It is worth noting that compared with ThT, the ZnO-Co_3O_4 NC–based sensor exhibits a higher sensitivity to the most toxic Aβ oligomer, which is significantly important for early diagnosis of AD.

Screening inhibitors of Aβ aggregation

Based on the different catalytic behaviors of ZnO-Co_3O_4 NCs in the presence of different forms of Aβ40 species, we also used the system to screen the inhibitors of Aβ40 aggregation (Fig. 6a). To verify our speculation, curcumin [34] and β-cyclodextrin [35], the well-known inhibitors of Aβ aggregation, were used for this proof-of-concept study. The catalytic activity of ZnO-Co_3O_4 NCs in the presence of curcumin or β-cyclodextrin pretreated Aβ40 samples was investigated. As shown in Fig. 6b, with increasing incubation time of Aβ40 with curcumin or β-cyclodextrin, the absorption of the systems at 652 nm was increased but not as high as that without inhibitors. A control experiment was also carried out to clarify the non-influence of the inhibitors on the peroxidase-like activity of ZnO-Co_3O_4 NCs (Fig. S10). All these results indicate that the process of Aβ fibrilization is inhibited by curcumin and β-cyclodextrin, leading to less amount of Aβ40 fibrils formed in the solution and then an enhanced suppression effects on the catalytic activity of ZnO-Co_3O_4 NCs. Due to the sensitivity of ZnO-Co_3O_4 NCs to Aβ oligomers, the ZnO-Co_3O_4 NC–based system may be suitable for screening molecules that inhibit the formation of Aβ oligomers. As demonstrated in Fig. 6b, although β-cyclodextrin could effectively inhibit the formation of Aβ40 fibrils, they had no effects on Aβ40 oligomerization, which was in consistence with the previous reports [35]. More interestingly, during the first 2 days of incubation, compared with Aβ40 peptide itself, the curcumin-treated sample exhibited less inhibitory effect on the catalytic activity of ZnO-Co_3O_4 NCs (Fig. 6), which may arise from the enriched formation of "off-pathway" soluble oligomers by curcumin [34]. The modulation of Aβ40 aggregation by curcumin and β-cyclodextrin was further demonstrated by TEM images (Fig. S11). Our system shows great

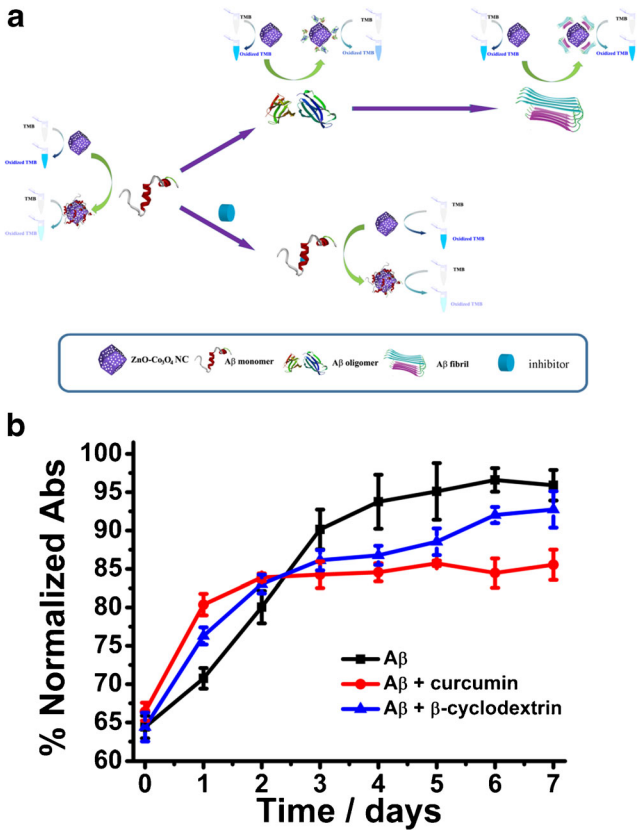

Fig. 6 **a** Schematic illustration of ZnO-Co_3O_4 NC–based strategy for sensing Aβ aggregates and screening of Aβ inhibitors. **b** Monitoring the inhibition effects of curcumin and β-cyclodextrin on Aβ aggregation by ZnO-Co_3O_4 NC–based assay. The concentration ratio of the inhibitor to Aβ was 1:1. The data of the absorption intensity was normalized to the maximum absorbance intensity of the sample without Aβ inhibitors

potential in screening inhibitors against the formation of Aβ oligomers, which is significantly important for AD treatment.

Actually, the strategy presented in this work for Aβ amyloidogenesis study and inhibitor screening is simple and does not require any complicated preparation methods. For the determination of Aβ monomer, due to the slight inhibition effect of Aβ oligomer on the catalytic activity of ZnO-Co_3O_4 NCs, our assay may not clearly distinguish Aβ monomer with a low concentration from oligomer at a very high concentration in complex samples. For seeking the good accuracy for evaluation of different Aβ species in complex samples in our further work, we assume to construct an aptasensor based on nanozyme to overcome this limitation.

Conclusions

Utilizing porous ZnO-Co_3O_4 NCs with peroxidase-like activity, a novel colorimetric assay for Aβ detection and amyloidogenesis study is developed. This assay, with a low detection limit (3.53 nM), was successfully used for the determination of Aβ monomer in rat CSF. On the basis of the different inhibition effects of monomeric and aggregated Aβ species on the catalytic activity of ZnO-Co_3O_4 NCs, this colorimetric assay has also been successfully applied for tracking the dynamic progress of Aβ aggregation and screening Aβ inhibitors. Significantly, compared with the commonly used thioflavin T fluorescence assay, this method presents higher sensitivity to Aβ oligomer at the very early assembly stage, which shows potential application in early diagnosis and therapy of AD. The study would shed light on the design of new diagnostic reagents for monitoring the disease progression and drug treatment efficacy in diseases linked to misfolded proteins.

Supplementary Information The online version contains supplementary material available at https://doi.org/10.1007/s00604-021-04705-4.

Funding Financial support was provided by the National Natural Science Foundation of China (Grant No. 21807024), the Youth Top-notch Talents Supporting Plan of Hebei Province, the Hundred Persons Plan of Hebei Province (E2018050012), Chunyu Project Outstanding Youth Fund of Hebei Medical University (No. CYYQ201904) and the Natural Science Foundation of Hebei Province (Grant No. B2020208035).

Compliance with ethical standards

Conflict of interest The authors declare that they have no conflicts of interest.

References

1. Panza F, Lozupone M, Logroscino G, Imbimbo BP (2019) A critical appraisal of amyloid-β-targeting therapies for Alzheimer disease. Nat Rev Neurol 15:73–88
2. Han X, He G (2018) Toward a rational design to regulate β-amyloid fibrillation for Alzheimer's disease treatment. ACS Chem Neurosci 9:198–210
3. Soto C, Pritzkow S (2018) Protein misfolding, aggregation, and conformational strains in neurodegenerative diseases. Nat Neurosci 21:1332–1340
4. Zhang Y, Ren B, Zhang D, Liu Y, Zhang M, Zhao C, Zheng J (2020) Design principles and fundamental understanding of biosensors for amyloid-β detection. J Mater Chem B 8:6179–6196
5. Lee D, Kim SM, Kim HY, Kim Y (2019) Fluorescence chemicals to detect insoluble and soluble amyloid-β aggregates. ACS Chem Neurosci 10:2647–2657
6. Zhou Y, Liu J, Zheng T, Tian Y (2020) Label-free SERS strategy for in situ monitoring and real-time imaging of Aβ aggregation process in live neurons and brain tissues. Anal Chem 92:5910–5920
7. Hu J, Zheng Q (2020) Applications of mass spectrometry in the onset of amyloid fibril formation: focus on the analysis of early-stage oligomers. Front Chem 8:324
8. Yu Y, Yin T, Peng Q, Kong L, Li C, Tang D, Yin X (2019) Simultaneous monitoring of amyloid-β (Aβ) oligomers and fibrils for effectively evaluating the dynamic process of Aβ aggregation. ACS Sens 4:471–478
9. Sebastiao M, Quittot N, Bourgault S (2017) Thioflavin T fluorescence to analyse amyloid formation kinetics: measurement frequency as a factor explaining irreproducibility. Anal Biochem 532:83–86
10. Li M, Zhao A, Ren J, Qu X (2017) N-Methyl mesoporphyrin IX as an effective probe for monitoring Alzheimer's disease β-amyloid aggregation in living cells. ACS Chem Neurosci 8:1299–1304
11. Lyu Z, Ding S, Zhang N, Zhou Y, Cheng N, Wang M, Xu M, Feng Z, Niu X, Cheng Y, Zhang C, Du D, Lin Y (2020) Single-atom nanozymes linked immunosorbent assay for sensitive detection of Aβ 1-40: a biomarker of Alzheimer's disease. Research 2020: 4724505
12. Qin J, Cho M, Lee Y (2019) Ferrocene encapsulated Zn zeolitic imidazole framework (ZIF-8) for optical and electrochemical sensing of amyloid-β oligomer and for the early diagnosis of Alzheimer's disease. ACS Appl Mater Inter 11:11743–11748
13. Lu K, Aung T, Guo N, Weichselbaum RR, Lin W (2018) Nanoscale metal-organic frameworks for therapeutic, imaging, and sensing applications. Adv Mater 30:1707634
14. Yang J, Wang C, Liu X, Yin Y, Ma Y-H, Gao Y, Wang Y, Lu Z, Song Y (2020) Gallium-carbenicillin framework coated defect-rich hollow TiO_2 as a photocatalyzed oxidative stress amplifier against complex infections. Adv Funct Mater 30:2004861
15. Liu X, Pan Y, Yang J, Gao Y, Huang T, Luan X, Wang Y, Song Y (2020) Gold nanoparticles doped metal-organic frameworks as near-infrared light-enhanced cascade nanozyme against hypoxic tumors. Nano Res 13:653–660
16. Zhang X, Li G, Wu D, Li X, Hu N, Chen J, Chen G, Wu Y (2019) Recent progress in the design fabrication of metal-organic frameworks-based nanozymes and their applications to sensing and cancer therapy. Biosens Bioelectron 137:178–198
17. Lv X, Yuan S, Xie L, Darke HF, Chen Y, He T, Dong C, Wang B, Zhang Y, Li J (2019) Ligand rigidification for enhancing the stability of metal-organic frameworks. J Am Chem Soc 141:10283–10293
18. Dang S, Zhu Q, Xu Q (2018) Nanomaterials derived from metal-organic frameworks. Nat Rev Mater 3:17075
19. Lan M, Guo R, Dou Y, Zhou J, Zhou A, Li J (2017) Fabrication of porous Pt-doping heterojunctions by using bimetallic MOF template for photocatalytic hydrogen generation. Nano Energy 33: 238–246
20. Zhao J, Dong W, Zhang X, Chai H, Huang Y (2018) FeNPs@Co_3O_4 hollow nanocages hybrids as effective peroxidase

mimics for glucose biosensing. Sens Actuators B Chem 263:575–584
21. Zhang M, Chen Z, Qin H, Yang X, Cao W, Liu S (2020) g-C_3N_4-Heme bound to amyloid β peptides: in-situ generation of the secondary co-reactant for dual-enhanced electrochemiluminescence assay of amyloid β detection. Electrochim Acta 361:137096
22. Ma Y, Yin L, Cao G, Huang Q, He M, Wei W, Zhao H, Zhang D, Wang M, Yang T (2018) Pt-Pd bimetal popcorn nanocrystals: enhancing the catalytic performance by combination effect of stable multipetals nanostructure and highly accessible active sites. Small 14:1703613
23. Iscen A, Brue CR, Roberts K, Kim J, Schatz GC, Meade TJ (2019) Inhibition of amyloid-β aggregation by cobalt(III) Schiff base complexes: a computational and experimental approach. J Am Chem Soc 141:16685–16695
24. Miura T, Suzuki K, Kohata N, Takeuchi H (2000) Metal binding modes of Alzheimer's amyloid β-peptide in insoluble aggregates and soluble complexes. Biochemistry 39:7024–7031
25. Asthana S, Hazarika Z, Nayak PS, Roy J, Jha S (2018) Insulin adsorption onto zinc oxide nanoparticle mediates conformational rearrangement into amyloid-like structure with enhanced cytotoxic propensity. Biochim Biophys Acta (BBA)-gen subj 1863:153–166
26. Zhang C, Ren J, Xing Y, Cui M, Li N, Liu P, Wen X, Li M (2020) Fabrication of hollow ZnO-Co_3O_4 nanocomposite derived from bimetallic-organic frameworks capped with Pd nanoparticles and MWCNTs for highly sensitive detection of tanshinol drug. Mater Sci Eng C Mater Biol Appl 108:110214
27. Zhao M, Huang J, Zhou Y, Pan X, He H, Ye Z, Pan X (2013) Controlled synthesis of spinel $ZnFe_2O_4$ decorated ZnO heterostructures as peroxidase mimetics for enhanced colorimetric biosensing. Chem Commun 49:7656–7658
28. Van Gool WA, Kuiper MA, Walstra GJ, Wolters EC, Bolhuis PA (1995) Concentrations of amyloid β protein in cerebrospinal fluid of patients with Alzheimer's disease. Ann Neurol 37:277–279
29. Deng C, Liu H, Zhang M, Deng H, Lei C, Shen L, Jiao B, Tu Q, Jin Y, Xiang L (2018) A light-up non-thiolated aptasensor for low-mass soluble amyloid-β40 oligomers at high salt concentrations. Anal Chem 3:1433–2402
30. Chen W, Gao G, Jin Y, Deng C (2020) A facile biosensor for Aβ40O based on fluorescence quenching of prussian blue nanoparticles. Talanta 216:120930
31. Liu L, Chang Y, Yu J, Jiang M, Xia N (2017) Two-in-one polydopamine nanospheres for fluorescent determination of beta-amyloid oligomers and inhibition of beta-amyloid aggregation. Sens Actuators B Chem 251:359–365
32. Kong L, Zhou X, Shi G, Yu Y (2020) Molybdenum disulfide nanosheets based fluorescent "off-to-on" probe for targeted monitoring and inhibition of β-amyloid oligomers. Analyst 145:6369–6377
33. Zhang Y, Meng S, Ding J, Peng Q, Yu Y (2019) Transition metal-coordinated graphitic carbon nitride dots as a sensitive and facile fluorescent probe for β-amyloid peptide detection. Analyst 144: 504–511
34. Thapa A, Jett SD, Chi EY (2016) Curcumin attenuates amyloid-β aggregate toxicity and modulates amyloid-β aggregation pathway. ACS Chem Neurosci 7:56–68
35. Wang Z, Chang L, Klein WL, Thatcher GRJ, Venton DL (2004) Per-6-substituted-per-6-deoxy β-cyclodextrins inhibit the formation of β-amyloid peptide derived soluble oligomers. J Med Chem 47:3329–3333